Journal of Physics: Conference Series

PAPER • **OPEN ACCESS**

Electric transport measurements on bulk, polycrystalline MgB_2 samples prepared at various reaction temperatures

To cite this article: A Wiederhold *et al* 2016 *J. Phys.: Conf. Ser.* **695** 012004

Electric transport measurements on bulk, polycrystalline MgB_2 samples prepared at various reaction temperatures

A Wiederhold[1], M R Koblischka[1], K Inoue[2], M Muralidhar[2], M Murakami[2], and U Hartmann[1]

[1]Institute of Experimental Physics, Saarland University, Campus C 6 3, D-66123 Saarbrücken, Germany.
[2]Superconducting Materials Laboratory, Department of Materials Science and Engineering, Shibaura Institute of Technology 3-7-5 Toyosu, Koto-ku, Tokyo 135-8548, Japan.

a.Wiederhold@physik.uni-saarland.de

Abstract. A series of disk-shaped, bulk MgB_2 superconductors (sample diameter up to 4 cm) was prepared in order to improve the performance for superconducting super-magnets. Several samples were fabricated using a solid state reaction in pure Ar atmosphere from 750 to 950 °C in order to determine the optimum processing parameters to obtain the highest critical current density as well as large trapped field values. Additional samples were prepared with added silver (up to 10 wt.-%) to the Mg and B powder. Magneto-resistance data and *I/V*-characteristics were recorded using an Oxford Instruments Teslatron system. From Arrhenius plots, we determine the TAFF pinning potential, U_0. The *I/V*-characteristics yield detailed information on the current flow through the polycrystalline samples. The current flow is influenced by the presence of pores in the samples. Our analysis of the achieved critical currents together with a thorough microstructure investigation reveals that the samples prepared at temperatures between 775 °C and 805 °C exhibit the smallest grains and the best connectivity between them, while the samples fabricated at higher reaction temperatures show a reduced connectivity and lower pinning potential. Doping the samples with silver leads to a considerable increase of the pinning potential and hence, the critical current densities.

1. Introduction

The metallic superconductor MgB_2, which was discovered 2001, has a critical temperature T_c of 39 K [1]. Even though this is low, compared to the T_c of high temperature superconductors, it posses several advantages. Due to its small coherence length it does not suffer from the weak link problem, wherefore it is possible to create cheap, large sized polycrystalline bulk samples [2]. Besides it has a high current transport capability [3] and strong trapped fields [4], which makes it to an ideal material for practical applications [5] like trapped field magnets. Therefore it is important to work out a cost-effective preparation method like simple sintering, which enables to produce large bulk samples with minimal cost [6-9]. In order to optimize the processing conditions, a series of samples was fabricated at various reaction temperatures ranging from 775 °C to 950 °C as described in Refs. [10,11]. For this

series of samples, the magnetic and electric properties were studied in detail to evaluate the critical current densities, the trapped fields, the effective flux pinning mechanism and the grain connectivity. Due to the porous structure of the sintered material, an additional set samples with an addition of silver (up to 10 wt.-%), which was already successfully used to improve the mechanical abilities and j_c values of (RE)BCO materials [13,14], were produced to improve the mechanical properties and the same measurements were performed there. The magnetic data were already presented in Ref. [12], so we focus in this contribution on the electric properties (resistance and *I/V*-characteristics) of this set of samples.

1. Experimental procedure

Polycrystalline MgB_2 samples were fabricated by using in-situ solid state reaction. Mg and B powders of high purity were pressed into pellets and sintered under argon atmosphere at temperatures from 775 to 950 °C. The silver doped samples were produced in the same way by adding up to 10 wt.-% of silver powder. Here the sintering temperature was selected to be 775 °C. More details on the sample preparation and their characterization are given elsewhere [10-12].

For the transport measurements, long bars with dimensions 1 × 2 × 8 mm^3, resulting in a distance of 5 mm between the voltage contacts, were cut from bulk MgB_2 samples using a diamond saw. The resistance was measured in four-probe configuration with a dc current of 30 mA applied perpendicular to the magnetic field direction. Thin copper wires of 100 µm in diameter were used as leads for low resistance contacts placed onto the samples by means of silver paste.

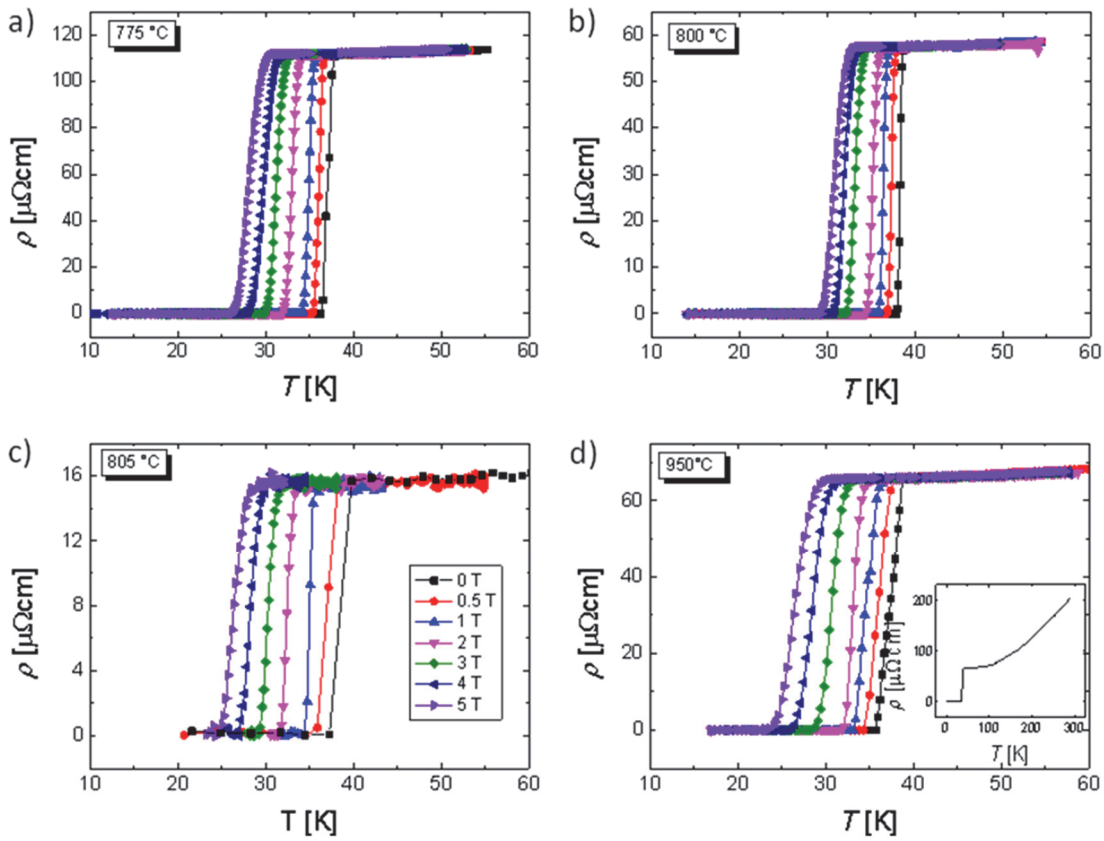

Figure 1. Electrical resistivity as function of temperature for different reaction temperatures measured in magnetic fields up to 5 T. The curves were obtained at a current of 30 mA. The inset in (d) presents the full curve from 4 to 300 K in zero field for the sample sintered at 950 °C.

Field steps of 1 T were used for the $R(T)$ measurements, and field steps of 0.25 T to collect the E-j-data. The magnetic field sweep rate was 0.7 T/min, and temperature steps of 0.25 K were applied.
The electric measurements were performed in an Oxford Instruments 10/12 T Teslatron cryostat in the temperature range 4 K – 300 K. The measurements were controlled by a MatLab program operating a stabilized current source (Keithley 2400) and a voltmeter (Keithley 2100 multimeter) [15].

2. Results and discussion

Figures 1 (a)-(d) present the resistivity data of the MgB_2 samples prepared at 775 °C, 800 °C, 805 °C and 950 °C. These samples were selected on the basis of the magnetic measurements performed in Refs. [5,7]. The first three samples were showing the best magnetic properties (critical current density, j_c, irreversibility fields and trapped fields), and the sample prepared at 950 °C showed strong pinning due to embedded MgB_4 particles [10,12].
All samples show a sharp superconducting transition which is shifting to lower values on increasing the external magnetic fields. With the electric resistivities in the normal conducting state, the geometrical connectivity can be estimated with $K = \Delta\rho_g/\Delta\rho$, while $\Delta\rho_g$ can be assumed to be 6.31 μΩcm for randomly orientated three dimensional samples and $\Delta\rho = \rho(300\text{ K}) - \rho(40\text{ K})$ [16]. The measured values for the normal conducting resistivities are shown in table 1. Figure 2 shows the calculated values for the connectivity as a function of the the sintering temperature. The connectivity shows an increase with growing processing temperature until a maximum at 805 °C, and then it decreases again, which reveals well coupled grains for sintering temperatures around 805 °C.

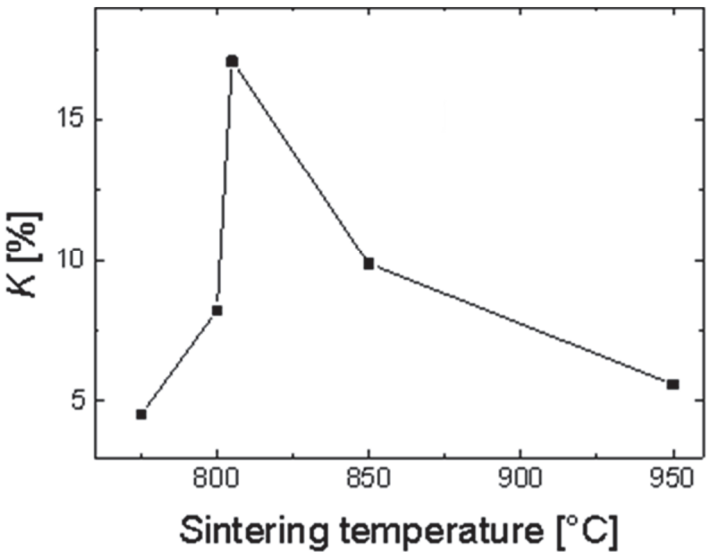

Figure 2. Connectivity as function of sintering temperature. The maximum at 805 °C indicates well coupled grains for process temperatures around this point.

The data can be converted into Arrhenius-plots by plotting the logarithm of the electric resistivity against the inverse temperature, which is shown in figures 3 (a)-(d). From the slopes of the linear parts, the TAFF pinning potential can be calculated [17]. The V-I curves of the samples sintered at 775 °C, 800 °C, 805 °C and 950 °C are presented in figures 4 (a)-(d). As in the case discussed above, the critical current density shifts to lower values with increasing magnetic fields. Also a change in the shape of the curves can be observed on increasing reaction temperature. These curves enable the pinning potential in the flux creep region to be calculated [18].

Sintering temperature [°C]	ρ(300 K) [μΩcm]	ρ(40 K) [μΩcm]	$\Delta\rho$ [μΩcm]
775	251	111	140
800	134	57	77
805	52	15	37
850	106	42	64
950	179	66	113

Table 1. Normal conducting resistivity at 300 and 40 K and the calculated phonon term resistivity $\Delta\rho$ for the samples sintered at different temperatures.

Figure 5 shows the TAFF pinning potential calculated from the resistance data (a) and the flux creep pinning potential calculated from the *V-I* curves. The TAFF pinning potentials show strong pinning centers for the samples sintered at around 805 °C which is in agreement with Ref. [19]. In this study magnetic measurements were performed on the same samples and the highest j_c value of about 250 kA/cm² was observed at a sintering temperature of 805 °C. The flux creep potentials show similar results.

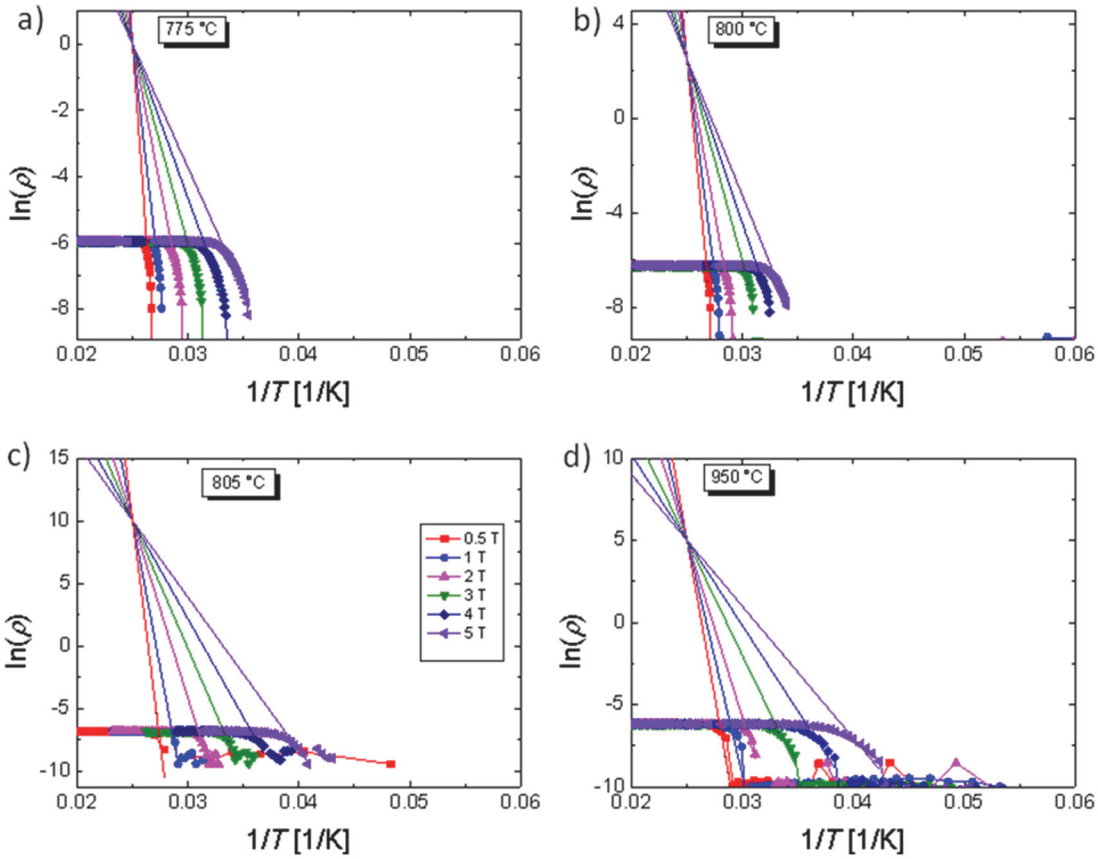

Figure 3. Arrhenius-plots of the data from figure 1. The TAFF pinning potential can be calculated with the slope of the linear parts. In order to find suitable fit parameters, it was assumed that the extrapolation of the slopes meet together in one common point at $1/T_c$, which is fixed from the $\rho(T,B = 0)$ data shown in figure 1.

Note that the smaller values occur due to much higher currents applied in the measurement. On the first sight, the weak pinning forces of the sample processed at 950 °C seem to be a contradiction to the results of Ref. [12], where magnetic measurements showed an increase of the pinning forces with increasing reaction temperature, but this gives important hints to the microstructure of the material.

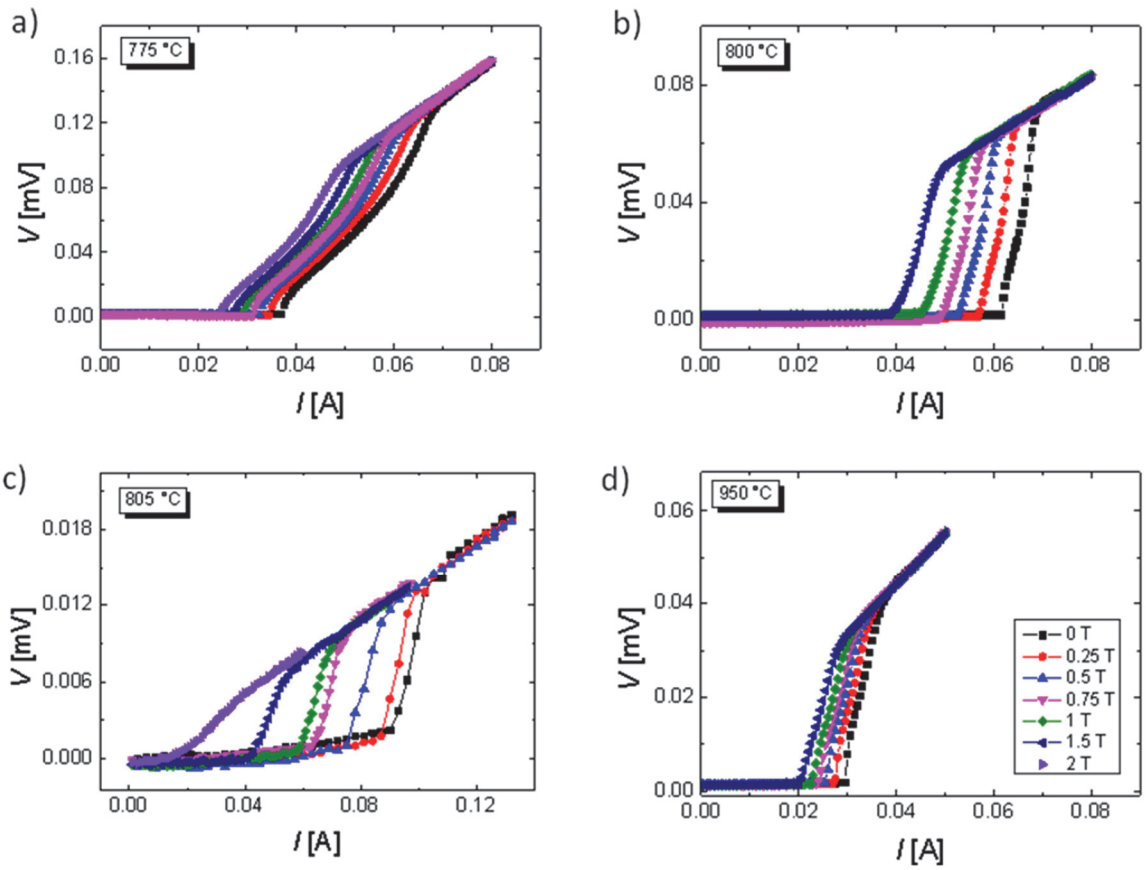

Figure 4. The voltage measured at 30 K as a function of current for different reaction temperatures in magnetic fields up to 2 T.

On increasing the reaction temperature, the number of point pinning centers, provided by MgB_4 inclusions, increases. But simultaneously the quality of the grain boundaries and therefore the intergrain connectivity decreases. Due to the different source of the shielding currents these currents are able to flow in single grains in the case of the magnetic measurements. Therefore, the sample sintered at 950 °C shows there a high pinning potential. In the electric measurements, the currents are forced to flow through the whole sample. This is the reason for the larger pinning forces of the samples sintered at around 805 °C in the case of the electric measurements due to a combination of strong point pinning centers provided by MgB_4 particles and a good intergrain connectivity.
Since the best process parameters for sintered MgB_2 samples were found at this point, one big disadvantage of these low cost samples remains. The material produced via the in-situ solid state reaction exhibits a density of just about 50% of the theoretically maximum density of MgB_2, which is low compared to other methods like spark plasma sintering [20]. This strongly requires an improvement of the mechanical properties of the resulting soft and porous samples. Therefore, silver-doped MgB_2 samples sintered at 775 °C (the optimum temperature found in Ref. [9]) were produced with silver contents ranging between 0 wt.-% and 10 wt.-%. In order to compare the electric and

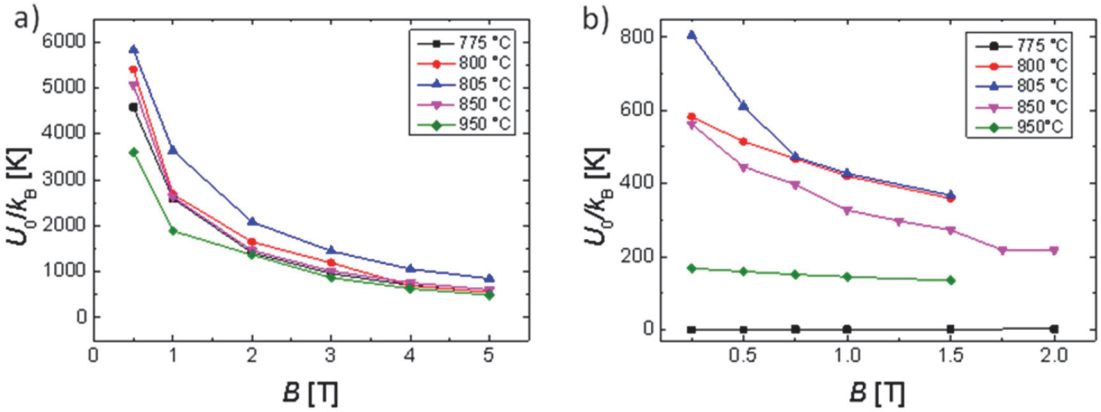

Figure 5. TAFF pinning potential (a) and flux creep pinning potential (b) as function of the magnetic field for various reaction temperatures at 30 K. In both cases, the sample sintered at 805 °C shows the highest value which indicates a combination of strong pinning centers and a good intergrain connectivity.

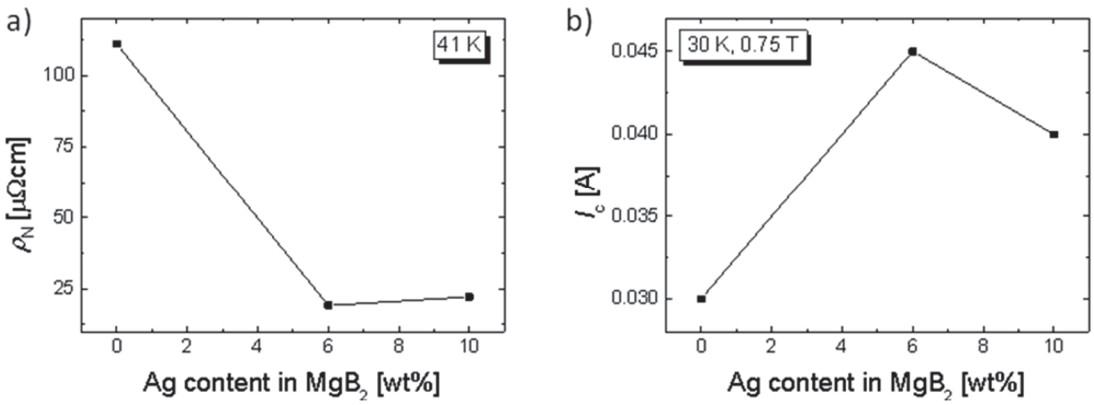

Figure 6. (a) Normal conducting electrical resistivity as function of Ag content taken at 41 K for the samples sintered at 775 °C. A decrease with silver doping is visible. (b) Critical current density as function of Ag content obtained at 0.75 T (30 K).

magnetic properties to the previous samples, the same transport measurements showed above were performed on these samples.

The electrical resistivities in the normal conducting state for the samples with silver contents of 0 wt.-%, 6 wt.-% and 10 wt.-%, which are obtained at 41 K, are shown in figure 6 (a). A decrease of the resistance with silver doping is clearly visible. The smallest value of 19 μΩcm is reached for an Ag content of 6 wt.-% of silver. Figure 6 (b) shows the critical current obtained at 0.75 T at 30 K. Higher values are reached with silver doping compared with the sample without silver. Also in this case, the highest value is reached for the sample with an Ag content of 6 wt.-%. The pinning potentials calculated from the resistivity and the *V-I* data are presented in figure 7. An increase of the TAFF pinning potential [figure 7 (a)] with silver doping is visible. This can be seen in the flux creep pinning potential as well. In both cases, the sample with an Ag content of 6 wt% shows the strongest pinning centers. These results can be explained with microstuctural observations in Ref. [11]. It was shown that silver doping leads to a formation of nanometer-sized $AgMg_3$ particles in the material, which can

deal as additional pinning centers and hence increase the critical currents and improve the pinning properties. The study shows that the highest values for j_c is observed for Ag contents of 4-6 wt% due to a homogenous distribution of these particles, which is in agreement with our observations. This clearly demonstrates that silver doping leads to an improvement of the magnetic [11] and electric properties but also the mechanical properties can be improved, which is shown in Ref. [11].

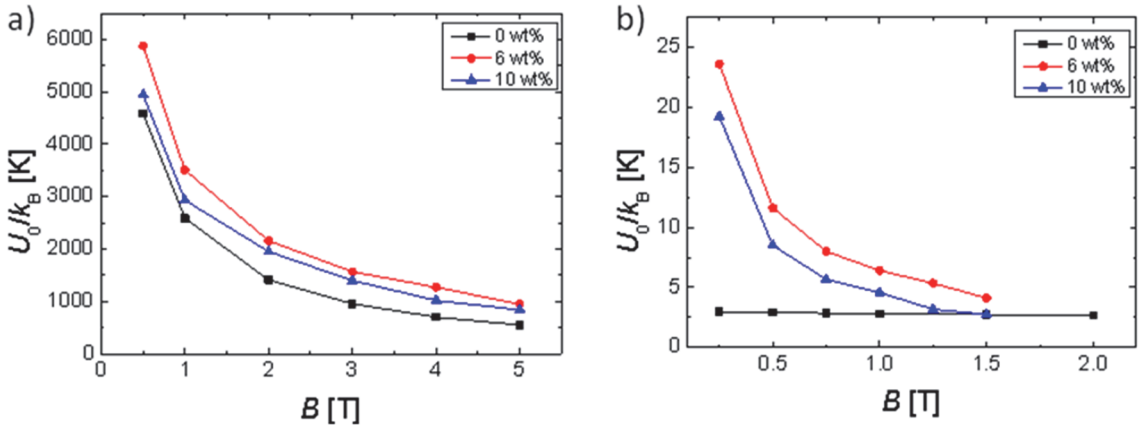

Figure 7. TAFF pinning potential (a) and flux creep pinning potential at 30 K (b) as function of the magnetic field for the different Ag contents. It is clearly visible that the silver addition improves the pinning centers in both cases. The highest potential is obtained at a silver content of 6 wt.-%.

Conclusions

To summarize, transport measurements were performed on various MgB_2 samples. The measurements reveal the best sintering temperature being around 805 °C for the low cost solid state reaction due a good intergrain connectivity and a high pinning potential. The properties of these samples can be improved further with silver doping which leads to stronger pinning, higher j_c values and higher trapped fields.

References

[1] Nagamatsu J, Nakagawa N, Muranaka T, Zenitani Y and Akimitsu J 2001 *Nature* **40** 1
[2] Moshchalkov V, Menghini M, Nishio T, Chen Q, Silhanek A, Dao V, Chibotaru L, Zhigadlo N and Karpinski J 2009 *Phys. Rev. Lett.* **102** 117001
[3] Muralidhar M, Inoue K, Koblischka M R, Tomita M and Murakami M 2014 *J. Alloys Compd.* **608** 102
[4] Yamamoto A, Ishihara A, Tomita M and Kishio K 2014 *Appl. Phys. Lett.* **105** 032601
[5] Tomsic M, Rindfleisch M, Yue J, McFadden K and Phillips J 2007 *J. Appl. Ceram. Technol.* **4** 3
[6] Buzea C and Yamashita T 2001 *Supercond. Sci. Technol*. **14** R115
[7] Glowacki B A, Majoros M, Vickers M, Evetts J E, Shi Y and McDougall I 2001 Supercond. Sci. Technol. **14** 193
[8] Naito T, Sasaki T and Fujishiro H 2012 *Supercond. Sci. Technol*. **25** 095012
[9] Muralidhar M, Ishihara A, Suzuki K, Fukumoto Y, Yamamoto Y and Tomita M 2013 *Physica C* **494** 85
[10] Muralidhar M, Inoue K, Koblischka M R, Tomita M and Murakami M 2014 *J. Alloy Compounds* **608** 102
[11] Muralidhar M, Inoue K, Koblischka M R, Murakami A and Murakami M 2015 *Adv. Eng. Mater*. **17** 831
[12] Koblischka M R, Wiederhold A, Muralidhar M, Inoue K, Hauet T, Douine B, Berger K, Murakami M and Hartmann U 2014 *IEEE Trans. Magn*. **50** 9000504

[13] Singh Y, Leu M J, Koepke K P, Van Voorhees E, Goudey G T, Winsley K and Shi D 1989 *J. Appl. Phys.* **66** 3154
[14] Mendoza E, Puig T, Varesi E, Carrillo AE, Plain J and Obrados X 2000 *Physica C* **334** 7
[15] Wiederhold A, Koblischka M R, Inoue K, Muralidhar M, Berger K, Douine B, Hauet T, Murakami M and Hartmann U 2016, in: Superconductivity: Todays and Tomorrows Applications, ed. Muralidhar M, NOVA Science Pub., Commack, NY, p. 269
[16] Yamamoto A, Shimoyama J, Kishio K and Matsushita T 2007 *Supercond. Sci. Technol.* **20** 658
[17] Lei H, Wang K, Hu R, Ryu H, Abexkoon M, Bozin E S and Petrovic C 2012 *Sci. Technol. Adv. Mater.* **13** 054305
[18] Brandt E H 2012 *J. Nanosci. Nanotechnol.* **12** 1201
[19] Kobayashi H, Muralidhar M, Koblischka M R, Inoue K and Murakami M 2015 *Phys Procedia* **65** 73
[20] Noudem J G, Aburras M, Bernstein P, Chaud X, Muralidhar M and Murakami M 2014 *J. Appl. Phys*. **116** 163916